THE JOURNAL OF BIOLOGICAL CHEMISTRY VOL. 287, NO. 51, pp. 42455–42468, December 14, 2012

Rab13 Small G Protein and Junctional Rab13-binding Protein (JRAB) Orchestrate Actin Cytoskeletal Organization during Epithelial Junctional Development*[S]

Received for publication, May 19, 2012, and in revised form, October 22, 21012 Published, JBC Papers in Press, October 24, 2012, DOI 10.1074/jbc.M112.383653

Ayuko Sakane[‡], Ahmed Alamir Mahmoud Abdallah[‡], Kiyoshi Nakano[‡§], Kazufumi Honda[¶], Wataru Ikeda[‖], Yumiko Nishikawa[**], Mitsuru Matsumoto[**], Natsuki Matsushita[‡‡], Toshio Kitamura[§§], and Takuya Sasaki[‡1]

From the [‡]Department of Biochemistry, Institute of Health Biosciences, Graduate School, and [§]Student Lab, Faculty of Medicine, University of Tokushima , Tokushima 770-8503, the [¶]Division of Chemotherapy and Clinical Research, National Cancer Center Research Institute, Tokyo 104-0045, the [‖]KAN Research Institute, Inc., Kobe 650-0047, the [**]Division of Molecular Immunology, Institute for Enzyme Research, University of Tokushima, Tokushima 770-8503, the [‡‡]Functional Genomics Core Laboratory, Ehime University Proteo-Medicine Research Center, Ehime 791-0295, and the [§§]Department of Hematopoietic Factor, Institute of Medical Science, University of Tokyo, Tokyo 108-8639, Japan

Background: The Rab13-JRAB system transports cell adhesion molecules.
Results: JRAB interacts with actinins and F-actin and spatiotemporally regulates actin dynamics via a conformational change that is dependent upon Rab13.
Conclusion: Rab13 and JRAB regulate reorganization of the actin cytoskeleton throughout epithelial junctional development from establishment to maturation of cell-cell adhesion.
Significance: The Rab13-JRAB system may simultaneously coordinate vesicle transport and actin cytoskeletal organization.

During epithelial junctional development, both vesicle transport and reorganization of the actin cytoskeleton must be spatiotemporally regulated. Coordination of these cellular functions is especially important, but the precise mechanism remains elusive. Previously, we identified junctional Rab13-binding protein (JRAB)/molecules interacting with CasL-like 2 (MICAL-L2) as an effector of the Rab13 small G protein, and we found that the Rab13-JRAB system may be involved in the formation of cell-cell adhesions via transport of adhesion molecules. Here, we showed that JRAB interacts with two actin-binding proteins, actinin-1 and -4, and filamentous actin via different domains and regulates actin cross-linking and stabilization through these interactions. During epithelial junctional development, JRAB is prominently enriched in the actin bundle at the free border; subsequently, JRAB undergoes a Rab13-dependent conformational change that is required for maturation of cell-cell adhesion sites. These results suggest that Rab13 and JRAB regulate reorganization of the actin cytoskeleton throughout epithelial junctional development from establishment to maturation of cell-cell adhesion.

Adhesion of cells to their neighbors or to the extracellular matrix is critical for the assembly of single cells into ordered multicellular tissues and organs (1, 2). Adhesion requires several components as follows: specific transmembrane adhesion molecules that mediate binding to an external surface; cytoskeletal filaments that attach to the cytoplasmic faces of the adhesion site; and a submembrane plaque that interconnects the two (3–6). A dense band of actin and myosin encircles epithelial cells in the plane of cell-cell junctions; this band plays a crucial role in the assembly and disassembly of cell-cell associations (7–9). During development, the assembly of spot-like primordial adherens junctions occurs in parallel with the formation of thick F-actin bundles at the free border (arcs), followed by maturation of the primordia into belt-like adherens junctions (10–12). The regulation of actin cytoskeletal organization must be spatiotemporally coordinated; many factors, including actin-binding proteins and signal transduction molecules, participate in this process. Among these factors, Rho family small G proteins play a prominent role in such epithelial actin dynamics; this role has been extensively studied for many years (5, 6, 13–16).

In this study, we focus on Rabs, another family of small G proteins. In eukaryotic cells, Rab proteins serve as molecular switches in the regulation of vesicular trafficking (17–19); they are localized to different compartments, where they control distinct transport systems and thereby coordinate the targeting of a wide range of molecules to their appropriate functional destinations. One can easily imagine that the logistics involved may contribute to the spatiotemporal regulation of actin cytoskeletal organization. However, to date there has been little direct evidence of such a contribution, and no important molecules have yet been identified. Previous studies, including our own, have shown that Rab13 is involved in the transport of cell adhesion molecules and thereby regulates cell-cell adhesion between epithelial cells

* This work was supported by Grant-in-aid for Scientific Research on Innovative Areas 2008–2012 from the Ministry of Education, Culture, Sports, Science and Technology (to T. S.), Grant-in-aid for Scientific Research 2009–2012 (to T. S.), and Grant-in-aid for Young Scientists 2008–2012 from the Japan Society for the Promotion of Science (to A. S.).
[S] This article contains supplemental Figs. 1 and 2 and Movie.
[1] To whom correspondence should be addressed. Tel.: 81-88-633-9223; Fax: 81-88-633-9227; E-mail: sasaki@basic.med.tokushima-u.ac.jp.

(20–24). Moreover, we have identified junctional Rab13-binding protein (JRAB)[2]/molecules interacting with CasL-like 2 (MICAL-L2) (hereafter, JRAB) as effector proteins of Rab13, and we have shown that JRAB is a key factor in this process (24, 25).

Furthermore, we have demonstrated that actinin-4 is a JRAB-binding partner (26). The actinin proteins are a family of four closely related gene products (27). Actinin-1 and actinin-4 are localized to stress fibers, cellular protrusions/leading edges, and cell adhesion sites in non-muscle cells (28). Both proteins have F-actin cross-linking activity and are thereby capable of regulating rearrangement of the actin cytoskeleton. Thus, JRAB may play a key role in mediating the cross-talk between vesicular trafficking via Rab13 and the remodeling of the actin cytoskeleton by well characterized actin-binding proteins. Here, we describe the roles of Rab13-JRAB in reorganization of the actin cytoskeleton, from establishment to maturation of cell-cell adhesions, and we discuss the mechanisms underlying the coordination of vesicular trafficking and reorganization of the actin cytoskeleton during epithelial junctional development.

EXPERIMENTAL PROCEDURES

Plasmid Construction—cDNAs encoding JRAB, JRABΔCC, and JRABΔCT were subcloned into pCIneo-HA. Each mutant was amplified by PCR, using pCIneo-Myc-JRAB as a template. For production of the GST- or His_6-tagged recombinant proteins, the coding sequences of JRAB CH+LIM (amino acids (aa) 1–260), CH (aa 1–138), LIM (aa 139–260), MID (aa 261–805), MID NL (aa 261–679), MID CL (aa 394–805), MID NS (aa 261–542), MID CS (aa 543–805), MID1 (aa 261–393), MID2 (aa 394–679), MID3 (aa 680–805), and C (aa 806–1009) were subcloned into pGEX6P-1 or pRSET-A. To generate EGFP constructs, JRAB and the mutants described above were subcloned into pEGFP-C1. To produce retrovirus-expressing GFP-tagged proteins, we generated pMX-EGFP from the pMX vector (29). cDNAs encoding wild-type Rab13 (Rab13WT) and the dominant-active and dominant-negative mutants (Rab13DA and Rab13DN) were also subcloned into pMX-EGFP. pCIneo-Myc-actinin-4 was generated as reported previously (26). Actinin-4 cDNAs were subcloned into pEGFP-C1 or pRSET-A. cDNA encoding actinin-1 was isolated by reverse transcription (RT)-PCR from a mouse brain cDNA library and then cloned into pCIneo-Myc, pEGFP-C1, or pRSET-A. All plasmids constructed in this study were sequenced using an ABI Prism 3100 genetic analyzer (Applied Biosystems).

Antibodies—Rabbit anti-JRAB and rabbit anti-actinin-4 antibodies were described previously (30, 31). Mouse anti-Myc antibody (clone 9E10) was produced from a hybridoma obtained from ATCC; mouse anti-hemagglutinin (HA) (clone 12CA5) and rat anti-HA (clone 3F10) were from Roche Diagnostics; mouse anti-GAPDH antibody was from Applied Biosystems; rabbit anti-GFP, mouse anti-GFP antibodies, and rhodamine-phalloidin were from Invitrogen; mouse anti-actinin-4 was from TransGenic Inc.; mouse anti-actinin-1 was from Abnova; and rabbit monoclonal antibody against actinin-1 was from Epitomics, Inc. Alexa 488- or Alexa 546-conjugated secondary antibodies and HRP-coupled secondary antibodies were obtained from Invitrogen and Jackson ImmunoResearch, respectively.

Cell Culture and Transfection—MTD-1A cells were a kind gift from Dr. S. Tsukita (Kyoto University, Kyoto, Japan). MTD-1A cells were cultured in Dulbecco's modified Eagle's medium (DMEM) with 10% fetal bovine serum (FBS), 100 units/ml penicillin, and 100 mg/ml streptomycin. HEK293 cells were cultured in DMEM with 5% FBS, 1 mM sodium pyruvate, 100 units/ml penicillin, and 100 mg/ml streptomycin. Both MTD-1A and HEK293 were maintained at 37 °C in a water-saturated atmosphere of 95% air and 5% CO_2. HEK293 cells were transfected using Lipofectamine 2000 transfection reagent (Invitrogen), and MTD-1A cells were transfected either using a Nucleofector device (Amaxa) or Lipofectamine 2000 transfection reagent.

Recombinant Retrovirus Infection—The pMX-EGFP vectors containing JRAB, Rab13, and their mutants were transfected into PLAT-E cells as described previously (32). After a 48-h transfection, each culture supernatant was collected and filtered through a 0.45-μm filter prior to infection. MTD-1A cells were infected either with each recombinant retrovirus separately or with a mixture. After a 48-h culture period, cells were subjected to further experiments.

Pulldown Assays—HEK293 cells were seeded at a density of 5×10^5 cells on 60-mm dishes and transfected the following day with 4 μg of each plasmid, using Lipofectamine 2000. After a 48-h incubation at 37 °C, cells were washed once and scraped from the dishes into phosphate-buffered saline (PBS). Cells were lysed in 300 μl of Buffer A (10 mM Tris-HCl, pH 8, 1 mM EDTA, 1% (w/v) Nonidet P-40, 150 mM NaCl, and 10 μM (*p*-amidinophenyl)methanesulfonyl fluoride). The resulting lysates were centrifuged at 4 °C for 5 min at 16,100 × *g*, and each supernatant was mixed with purified GST-JRAB mutant protein bound to glutathione-Sepharose 4B beads (GE Healthcare) and incubated for 90 min at 4 °C. The beads were then washed with Buffer A three times and resuspended in SDS sample buffer. Comparable amounts of the proteins that remained associated with the beads were separated by SDS-PAGE. The fraction of Myc-actinin-1 or -actinin-4 bound to the affinity column was determined by immunoblotting using an anti-Myc antibody (9E10).

Immunoprecipitation—Forty eight hours after transfection, HEK293 cells were washed once and scraped from the dishes into PBS. The cells were lysed in 300 μl of Buffer A, and the resulting lysates were centrifuged at 4 °C for 5 min at 16,100 × *g*. An aliquot of the supernatant was saved and used to verify the expression of the indicated proteins. The rest of the supernatant was mixed with anti-HA monoclonal antibody (12CA5) bound to protein G-Sepharose FF beads (GE Healthcare) and incubated for 90 min at 4 °C. The beads were then washed with Buffer A three times and resuspended in SDS sample buffer. The immunoprecipitates were subjected to immunoblotting using anti-HA (3F10), anti-Myc (9E10), or anti-GFP antibody.

[2] The abbreviations used are: JRAB, junctional Rab13-binding protein; MICAL-L2, molecules interacting with CasL-like 2; PLA, proximity ligation assay; CH, calponin homology; CC, coiled-coil; PM, plasma membrane; CT, C-terminal; aa, amino acid; TER, transepithelial electrical resistance; NCM, normal Ca^{2+} medium; LCM, low Ca^{2+} medium; MID, middle; full, full-length; TJ, tight junction.

Immunocytochemistry—MTD-1A cells were seeded at a density of 2×10^5 cells on coverslips in individual 35-mm dishes. The cells were transfected the following day with various cDNA-expressing plasmids. After a 48-h incubation, the cells were fixed with 1 or 4% formaldehyde in PBS for 20 min at room temperature. In the case of cells transduced with the recombinant retroviruses, cells were seeded under the same conditions and fixed the following day. After washing with PBS, cells were incubated in 5% donkey serum and 0.1% Triton X-100 in PBS for 30 min. Next, cells were incubated with primary antibodies for 1 h, followed by incubation with Alexa 488- or Alexa 546-conjugated secondary antibodies for 1 h. F-actin was labeled with rhodamine-phalloidin. Samples were mounted on glass slides and observed using an LMS Pascal confocal scanning microscope (Carl Zeiss), an A1 confocal laser scanning microscope (Nikon), or an N-SIM super-resolution microscope (Nikon).

shRNA-mediated Knockdown of JRAB Expression—The 19-mer shRNA pSuper.retro.puro plasmids (Oligoengine, Halo-Bio RNAi Therapeutics, Inc.) targeting mouse JRAB were used to knock down endogenous JRAB expression in MTD-1A cells. Two shRNA-containing expression cassettes, targeting different regions of JRAB mRNA (5′-GGACGGTTCAGGAGGCAAA-3′ and 5′-GGCTGAAGCCTGTGGATAA-3′), were used. A control shRNA, which did not match any known mouse gene, was used as a negative control. To produce retroviruses, the JRAB and control shRNA plasmids were transfected into PLAT-E cells as described above.

Immunoblotting—Cell lysates or immunoprecipitates were separated by SDS-PAGE, transferred to Immobilon-P membranes (Merck), and blocked for 1 h in Tris-buffered saline containing 5% nonfat dry milk. After incubation with specific primary antibodies for 1 h, and then with HRP-coupled secondary antibodies for 1 h, immunoreactive proteins were visualized using an ECL Plus kit (GE Healthcare).

Two-hybrid Screening—JRAB-MID NL was cloned into the yeast two-hybrid bait vector pGBDU-C1 (33). A mouse 11-day-old embryo cDNA library in the yeast two-hybrid prey vector pACT2 was purchased from Clontech. The yeast strain PJ69-4A (*MATa trp1-901 leu2-3,112 ura3-52 his3-200 gal4Δ gal80Δ GAL2-ADE2 LYS2::GAL1-HIS3 met2::GAL7-lacZ*) was sequentially transformed with pGBDU-JRAB-MID NL and the mouse 11-day-old embryo cDNA library. Two-hybrid screening was performed and evaluated as described previously (24–26).

In Vitro F-actin Binding and Cross-linking Assays—For the F-actin binding assay, F-actin (Cytoskeleton, Inc.) (23 μM stock) was incubated with purified recombinant proteins for 30 min at 24 °C. The recombinant proteins were pre-cleared by centrifugation at 125,000 × *g* for 1 h at 4 °C prior to each experiment. The mixture was ultracentrifuged at 125,000 × *g* for 90 min at 24 °C, and the supernatant and the pellet were subjected to SDS-PAGE followed by Coomassie Brilliant Blue staining. For the F-actin cross-linking assay, the proteins were incubated with F-actin under the same condition as for the F-actin binding assay and subsequently centrifuged at 16,000 × *g* for 10 min. Equal amounts of supernatant and pellet samples were analyzed by SDS-PAGE and Coomassie Brilliant Blue staining. The amounts of each recombinant protein or actin in the supernatant and pellet were quantified using Image Lab software in the Gel Doc EZ system (Bio-Rad). Differences among groups were tested with the Student's *t* test, or a one-way analysis of variance, followed by Scheffe's post hoc test, was used. Differences were assessed with a two-sided test and considered significant at the $p < 0.05$ level.

F-actin Polymerization and Depolymerization Assays—Pyrene-labeled actin in G-buffer (Cytoskeleton, Inc.) was polymerized by adding 10× Actin Polymerization buffer (0.25× final concentration) and incubated at room temperature for 1 h. Depolymerization was carried out according to the manufacturer's instructions. Briefly, to induce depolymerization, pyrene-labeled F-actin was diluted to the critical concentration (0.4 μM) with G-buffer. The fluorescence decrease was recorded over the course of 3600 s using a Varioskan Flash multimode reader (Thermo Fisher Scientific).

Bacterial Production of Recombinant Proteins—GST fusion proteins were expressed in *Escherichia coli* strain DH5α cultured in the presence of 0.1 mM isopropyl β-D-thiogalactopyranoside. Bacteria were resuspended in Buffer B (20 mM Tris-HCl, pH 8.0, 1 mM EDTA, 1 mM dithiothreitol) and lysed by sonication; cellular debris was removed by centrifugation for 60 min at 100,000 × *g*. The resulting supernatant was applied to a glutathione-Sepharose 4B column (GE Healthcare). The pass-through fraction was applied a second time to the same column. The column was washed with Buffer B, and the GST fusion proteins were eluted in Buffer C (50 mM Tris-HCl, pH 8.0, 10 mM reduced glutathione). The eluted proteins were detected by electrophoresis and Coomassie Brilliant Blue staining (data not shown). The His_6-tagged proteins were expressed in *E. coli* strain BL21 (DE3) pLysS (Novagen, EMD Biosciences, Inc.) and cultured in the presence of 0.1 mM isopropyl β-D-thiogalactopyranoside. Recombinant proteins were purified using TALON metal affinity resin (Clontech) according to the manufacturer's recommendations with slight modifications.

Cell Sorting, Wound Healing, and Live Cell Imaging—MTD-1A cells expressing GFP-JRAB were selected based on fluorescence intensity and isolated by single-cell sorting on a BD FACSAriaII (BD Biosciences). Cells were seeded at a density of 4×10^5 cells on glass-based dishes (Matsunami) and grown to confluence for 48 h. Wound edges were generated by scratching with a pipette tip. After scratching, cells were washed three times with PBS and re-fed with culture media. Live cell images were obtained using a BioStation IM (Nikon).

Duolink in Situ PLA—Duolink *in situ* proximity ligation assay (PLA) reagents were obtained from Olink Bioscience. MTD-1A cells expressing GFP-JRAB or GFP-JRABΔCC were fixed with acetone/methanol for 3 min and then blocked in Duolink Blocking stock ×1. Following incubation with primary antibody for 1 h at room temperature, and secondary antibody conjugated with oligonucleotide for 2 h, assays were performed according to the manufacturer's instructions. The specimens were observed using an LMS Pascal confocal scanning microscope (Carl Zeiss).

Ca^{2+} Switch Assay—A Ca^{2+}-switch assay was performed as described previously (24–26). Briefly, MTD-1A cells were grown in DMEM with 10% FBS (normal Ca^{2+} medium, NCM) and were sequentially incubated in Ca^{2+}-free minimal essential medium containing 5 mM EGTA without FBS (low Ca^{2+}

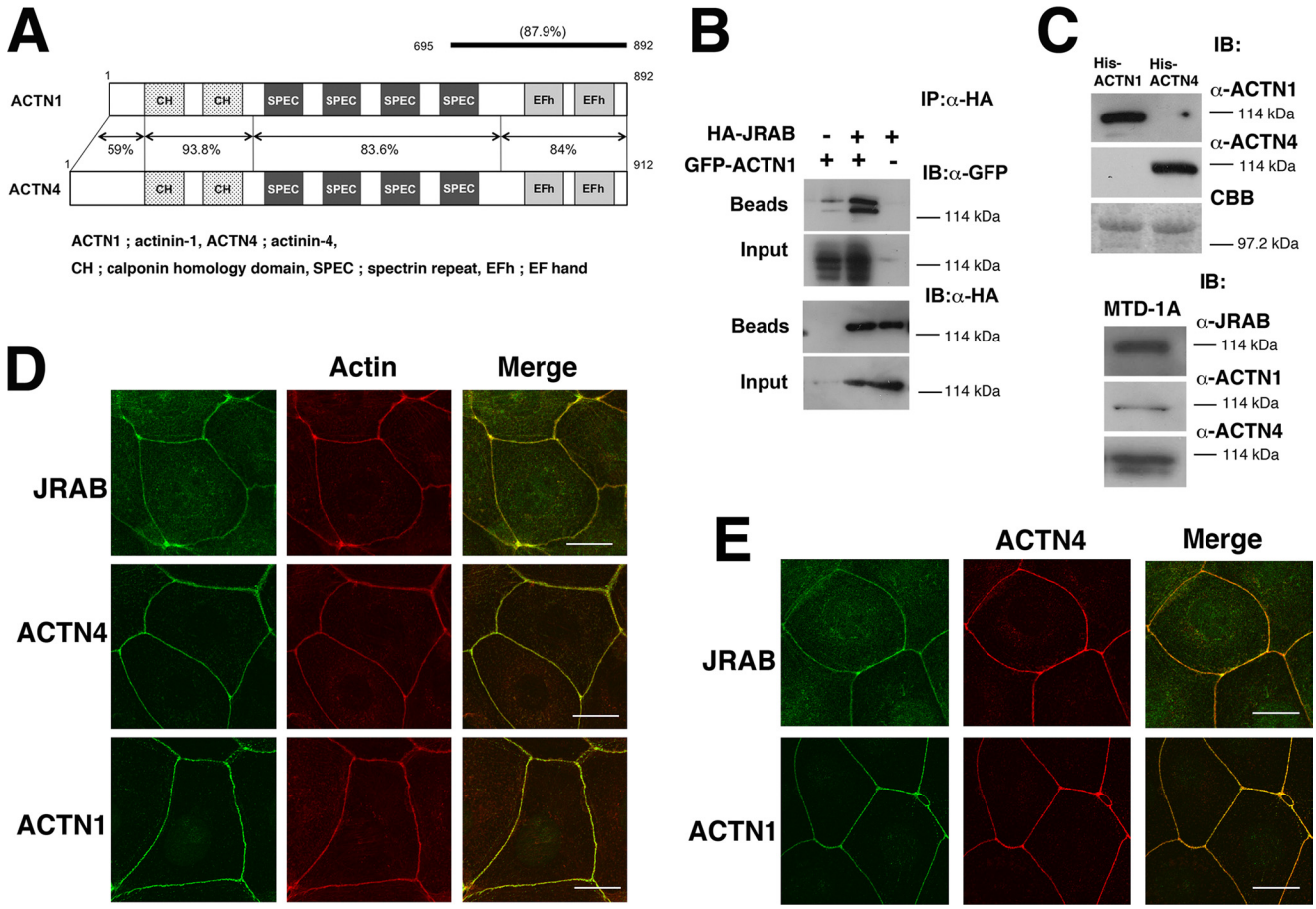

FIGURE 1. **Identification of actinin-1 as a JRAB-binding partner.** *A,* structures of mouse actinin-1 and actinin-4. *Numbers* represent amino acid positions and identities between actinin-1 and -4. A *line* indicates proteins encoded by the positive clones in the yeast two-hybrid system. *B,* HEK293 cells expressing HA-JRAB and GFP-actinin-1 were immunoprecipitated (*IP*) with anti-HA antibody and subjected to immunoblotting (*IB*) analysis. *C,* specificity of actinin-1 and actinin-4 antibodies. His_6-actinin-1 and -actinin-4 were subjected to SDS-PAGE, followed by immunoblotting with anti-actinin-1 and -actinin-4 antibodies (*top panel*). Using the same antibodies, we confirmed that actinin-1 and actinin-4 are expressed in MTD-1A cells (*bottom panel*). *CBB*, Coomassie Brilliant Blue. *D,* MTD-1A cells were double-stained with rhodamine-phalloidin and either anti-JRAB, anti-actinin-1, or anti-actinin-4 antibody. *Bar,* 20 μm. *E,* colocalization of JRAB, actinin-1, and actinin-4 at cell-cell adhesion sites in MTD-1A cells. MTD-1A cells were double-stained with anti-actinin-4 and either anti-JRAB or anti-actinin-1 antibodies. *Bar,* 20 μm. The results shown are representative of at least three independent experiments.

medium, LCM) for the indicated time to observe the junctional disassembly. For pharmacological modulation of the cytoskeleton, the cells were preincubated for 1 h with inhibitors in NCM, followed by 30-min incubation in LCM containing the same concentration of inhibitors. For analysis of junctional assembly, the cells were incubated in NCM for the indicated time after a 3-h incubation in LCM. For pharmacological modulation of assembly, the cells were subjected to a 3-h incubation in LCM and then preincubated for 30 min with inhibitors in LCM, followed by transferring into NCM containing the same concentration of inhibitors.

Measurement of Transepithelial Electrical Resistance (TER)—MTD-1A cells were replated onto Transwell filters (a polycarbonate membrane with 0.4-μm pore size), functioning as instant confluent monolayers, and cultured. TER was measured directly from the cultured medium as described previously (24–26).

RESULTS

JRAB Interacts with Actinin-1 as Well as Actinin-4—JRAB consists of three main domains as follows: the N-terminal domain, containing the CH and LIM subdomains; the C-terminal coiled-coil (CC) domain; and the MID domain connecting LIM and CC (25). In epithelial MTD-1A cells, JRAB is present both at cell-cell contact regions of the plasma membrane (PM) and in the cytosol. We also demonstrated that the N-terminal portion of MID (NL, aa 261–679; previously named MN) is the PM-targeting domain (26). To identify JRAB-binding proteins that contribute to this PM targeting activity, we performed a yeast two-hybrid screening using NL as bait. We reported previously that actinin-4 is one of the NL-binding proteins discovered in this screen (26). Another group of clones contained partial sequences identical to the cDNA of actinin-1. Actinin-1 and actinin-4 share more than 80% amino acid identity, and their overall domain organizations are very similar (Fig. 1*A*). We also confirmed the interaction of actinin-1 with JRAB by immunoprecipitation assay (Fig. 1*B*). Using antibodies specific for actinin-1 and actinin-4, we confirmed that both proteins are expressed in MTD-1A cells (Fig. 1*C*). Both of these proteins as well as JRAB can be detected at the rhodamine-phalloidin-positive cell-cell contact regions of the PM (Fig. 1*D*); in confluent cultures, they colocalize in these regions (Fig. 1*E*).

Localization of JRAB at the Plasma Membrane in Actinin-dependent and -independent Manner—In pulldown assays using GST-tagged truncated mutants of JRAB, Myc-actinin-1 was

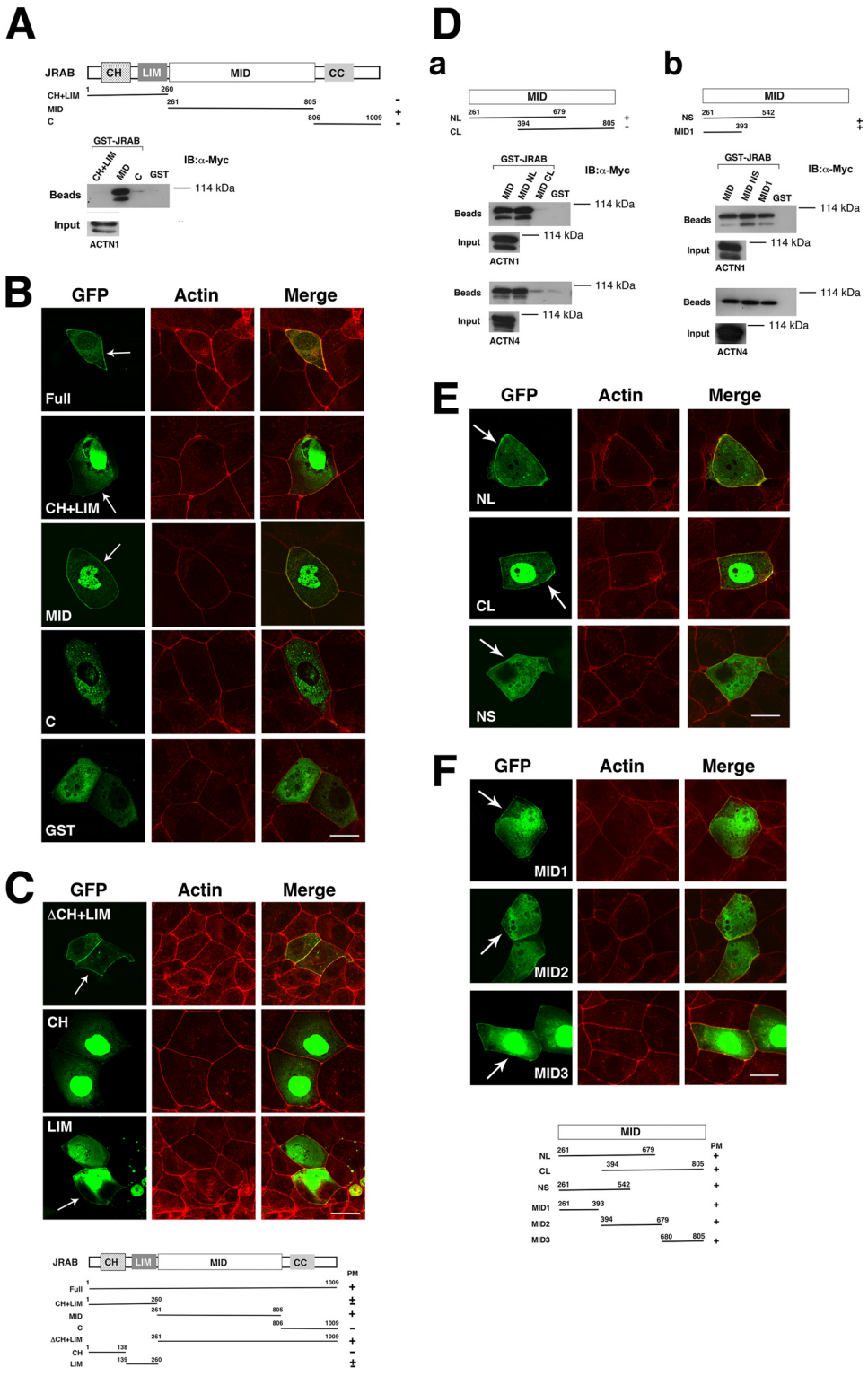

FIGURE 2. **Distinct regions of JRAB MID are required for the binding of actinin-1/4 and PM targeting.** *A* and *D,* HEK293 cells expressing Myc-actinin-1 or -actinin-4 were lysed and subjected to pulldown assays using GST proteins. The bound proteins were detected by immunoblotting (*IB*). The schema indicates each domain and its binding to actinins. *B, C, E,* and *F,* MTD-1A cells expressing GFP-tagged full-length or deletion mutants of JRAB were fixed and processed for double fluorescence. *Arrows* indicate PM targeting. The schema indicates each domain and its PM targeting activity. *Bar,* 20 μm. The results shown are representative of at least three independent experiments.

associated with GST-MID, but not with GST-CH+LIM, GST-C, or GST (Fig. 2*A*), as described previously for actinin-4 (26). Therefore, we predicted that JRAB might be targeted to the actin-based PM via actinin-1/4. To test this possibility, we expressed GFP-JRAB full-length (full), GFP-JRAB CH+LIM, GFP-JRAB MID, GFP-JRAB C, or GFP-GST in MTD-1A cells. We found that GFP-JRAB-full and MID proteins were targeted to the PM (Fig. 2*B*), consistent with our previous observations

using Myc-tagged constructs (26). Some GFP-CH+LIM was also observed at the PM, as well as in the cytosol, although its concentration was lower than that of GFP-JRAB-full or MID (Fig. 2*B*). GFP-C was detected in a vesicle-like structure in the cytoplasm but not at the PM (Fig. 2*B*). GFP-GST, analyzed as a control, was distributed throughout the cytoplasm. GFP-LIM was partially localized to the PM, like GFP-CH+LIM, but GFP-CH was not (Fig. 2*C*). However, GFP-tagged JRAB lacking CH+LIM was clearly detected at the PM (Fig. 2*C*), suggesting that the CH+LIM domain exhibits the PM targeting activity of JRAB, but only weakly compared with MID, and it may not be essential.

We next examined whether the cellular localization of JRAB MID is determined by its interaction with actinins. For this purpose, we tried to narrow down the region responsible for binding of JRAB MID to actinins. To this end, we prepared GST-tagged deletion mutants of MID and subjected them to pulldown assays. Myc-actinin-1/4 bound to the NL region, but it did not bind to the C-terminal region, CL (aa 394–805) (Fig. 2*D, panel a*). Myc-actinin-1/4 also bound to other truncation mutants, GST-NS (aa 261–542) and -MID1 (aa 261–393) (Fig. 2*D, panel b*), indicating that the minimal region of JRAB necessary for actinin-1/4-binding resides between amino acids 261 and 393. We next expressed these mutants in MTD-1A cells. GFP-NL and -NS localized to the PM (Fig. 2*E*), as we predicted. Surprisingly, GFP-CL localized to the PM (Fig. 2*E*), suggesting that JRAB can be translocated to the PM even in the absence of actinins.

To determine which part of CL is the primary determinant of the interaction, we expressed GFP-MID2 (aa 394–679) and GFP-MID3 (aa 680–805) as well as GFP-MID1. All mutants localized to the PM to a similar extent (Fig. 2*F*). Based on our previous data, we concluded that JRAB associates with F-actin at the PM via interaction with actinin-4, and probably actinin-1 as well. However, there is a strong possibility that JRAB might also interact with F-actin in an actinin-independent manner.

JRAB Directly Interacts with Filamentous Actin—We next performed high speed cosedimentation assays to determine whether JRAB binds directly to F-actin. JRAB CH+LIM and JRAB MID were found exclusively in the pellet fraction, whereas large amounts of JRAB-C and GST were detected in the supernatant fraction (Fig. 3*A, panel a*). In the CH+LIM domain, the LIM domain bound to F-actin, whereas the CH domain failed to bind (Fig. 3*A, panel b*). In the MID domain, MID-NS, -CS (aa 543–805), and -CL co-fractionated with F-actin; however, the affinity of MID-NS for F-actin is weaker than that of MID-CS or -CL (Fig. 3*A, panel b*). MID1, which contains the actinin-1/4-binding site, remained almost exclusively in the supernatant fraction (Fig. 3*A, panel b*). Both MID2 and MID3 bound to F-actin, but MID3 was pelleted less efficiently than MID2. These observations indicate that JRAB itself has actin binding activity and that the actinin-1/4-binding site in the MID domain is not essential for this interaction.

JRAB Stimulates the Cross-linking of F-actin and Suppresses the Depolymerization of F-actin—To analyze the effect of JRAB on F-actin cross-linking, we performed low speed cosedimentation assays. The addition of JRAB CH+LIM or JRAB MID significantly enhanced the formation of F-actin bundles relative to JRAB C or GST alone (Fig. 3*B, panel a*). In the CH+LIM domain, F-actin cross-linking ability was preserved in the LIM domain (albeit significantly reduced) but not in the CH domain (Fig. 3*B, panel b*). MID-CL and MID2 exhibited actin cross-linking activity similar to that of the MID domain, whereas MID1 and MID3 did not (Fig. 3*B, panel b*).

Next, we monitored polymerization by following the fluorescence of pyrene-labeled actin, to determine whether JRAB affects actin assembly. No effect could be observed in the presence of any domain (supplemental Fig. 1*A*); therefore, JRAB is likely not essential for actin polymerization. Consistent with this, the CH+LIM, MID, and C domains all failed to bind G-actin in an actin monomer pulldown assay (supplemental Fig. 1*B*).

We further analyzed the effect of JRAB on depolymerization by monitoring fluorescence intensity. In the presence or absence of GST-MID, GST-C, or GST, fluorescence intensity decreased in a time-dependent manner, as a result of dilution-induced F-actin depolymerization (Fig. 3*C, panel a*). In contrast, after addition of GST-CH+LIM, the fluorescence intensity remained nearly stable over time. LIM weakly stabilized F-actin, but CH did not (Fig. 3*C, panel b*). The observation that LIM is less efficient than CH+LIM is consistent with the actin-cross-linking experiments described above. We conclude that the two domains must cooperate to express their full actin-cross-linking and -stabilizing capabilities.

Accumulation of JRAB at Thick F-actin Bundles at the Free Border—As described previously (25) and above, in MTD-1A cells JRAB localizes to cell-cell adhesion sites, where cortical actin accumulates. During epithelial junctional development, the qualities of F-actin continue to dramatically change until adjacent cells contact each other and complete cell-cell adhesion. Prior to cell-cell contact, we observed that bundles of F-actin were prominent at free edges of the cells, relative to cell-cell adhesion sites (Fig. 4*A*). Furthermore, JRAB also prominently accumulated at thick F-actin bundles at the free border (Fig. 4*A*, *dots*). To examine whether JRAB is involved in the formation of the bundles at the free border, we generated JRAB-knockdown cells (Fig. 4*B*). Knockdown of JRAB induced the loosening of F-actin bundles along the free border relative to control cells (Fig. 4*B*, *arrows* and *dots*). This change in the qualities of F-actin can be more clearly observed in a super-resolution image (Fig. 4*C*). Together, these observations support the idea that JRAB enhances the accumulation of F-actin bundles, especially along the free border, at the early stage of junctional development.

Change of JRAB Behavior during Epithelial Junctional Development—We next examined the dynamics of JRAB in response to changes in the qualities of F-actin during epithelial junctional development. For this purpose, we prepared MTD-1A cells expressing GFP-JRAB. At the early stage of junctional development, GFP-JRAB localized along the free border at sites where accumulation of F-actin bundles could be observed, similar to endogenous JRAB (Fig. 5*A, panel a, dots*; see Fig. 4*A*). After the free edges of adjacent cells made contact, the thick F-actin bundles were converted into thin cortical actin bundles, resulting in well developed cell-cell adhesion (Fig. 5*A, panels b* and *c, arrows*). The accumulation of GFP-JRAB weakened concomitantly with the deceleration of F-actin bundling

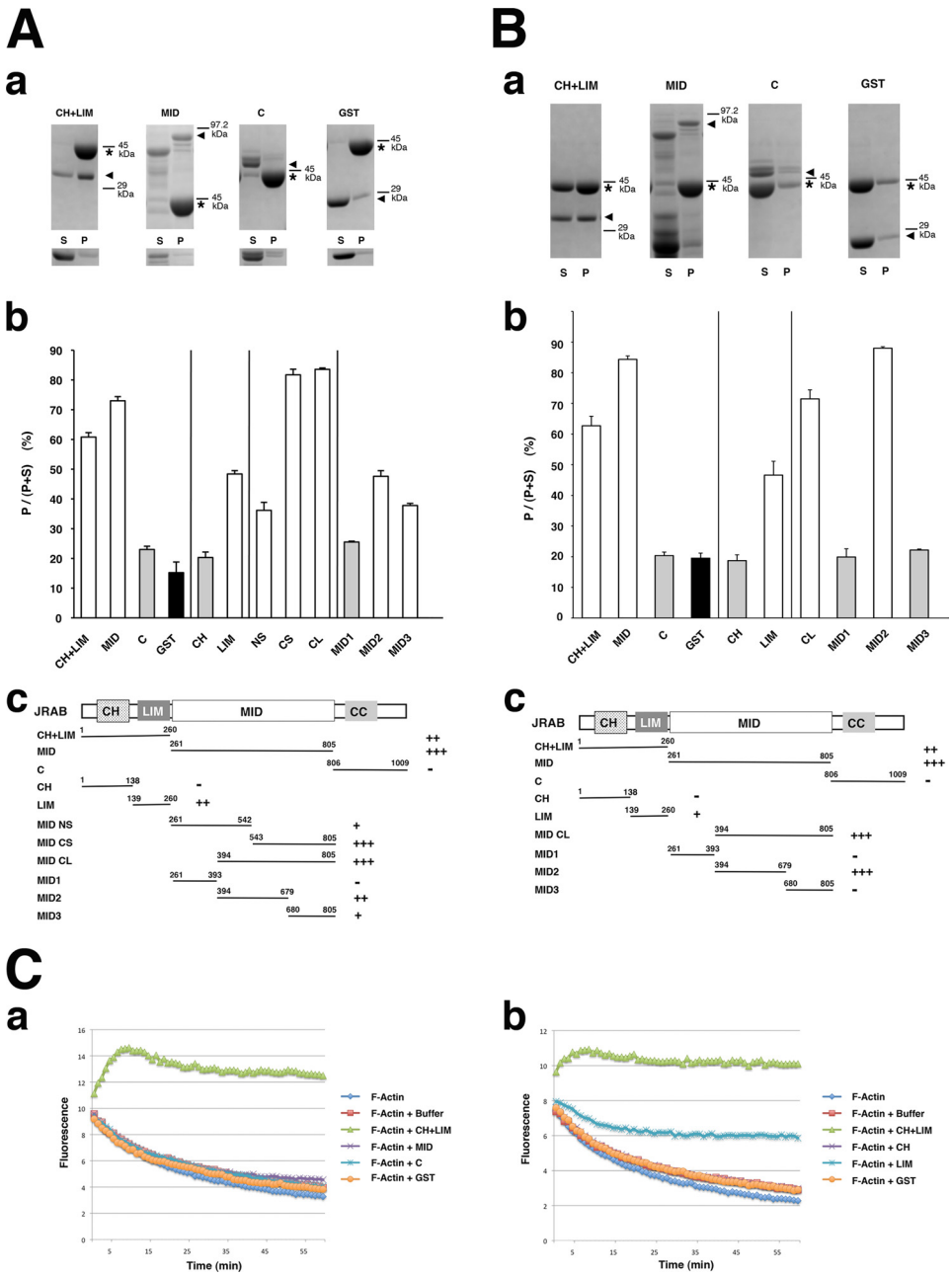

FIGURE 3. **JRAB directly binds to F-actin, induces cross-linking, and inhibits depolymerization of F-actin.** *A, panel a,* each recombinant protein was incubated with F-actin and centrifuged at 125,000 × *g*. An aliquot of the pellet (*P*) and supernatant (*S*) was subjected to SDS-PAGE, followed by Coomassie Brilliant Blue staining. *Top panels,* presence of F-actin; *bottom panels,* absence of F-actin. *Asterisks*, actin; *arrowheads*, recombinant proteins. *Panel b, graph* shows the ratio of each recombinant protein in the pellet *versus* total recombinant protein in the pellet and supernatant ($P/(P + S)$). *Black bar,* the negative control (GST); *open bars*, the proteins with F-actin-binding activity; *gray bars*, the proteins with no significant F-actin-binding activity. *Panel c,* schema indicates the ability of each protein to bind to F-actin. *B,* F-actin cross-linking activity of JRAB. *Panel a,* indicated recombinant proteins were incubated with F-actin and centrifuged at 16,000 × *g* to separate the pellet (*P*) and supernatant (*S*). *Asterisks*, actin; *arrowheads*, recombinant proteins. *Panel b, graph* shows the ratio of each recombinant protein in the pellet *versus* total recombinant protein in the pellet and supernatant ($P/(P + S)$). *Black bar,* the negative control (GST); *open bars*, the proteins with F-actin cross-linking activity; *gray bars*, the proteins with no significant cross-linking activity. *Panel c,* schema indicates the ability of each protein to cross-link F-actin. *C,* effect of JRAB on actin depolymerization. *Panels a* and *b,* indicated recombinant proteins were incubated with pyrene-labeled F-actin diluted to the critical concentration, and fluorescence was monitored using a spectrofluorometer. The results shown are representative of at least three independent experiments.

(Fig. 5*A*, *panel d, arrowheads*). To further elucidate this behavior of GFP-JRAB, we performed wound-healing assays and acquired time-lapse images during wound closure (Fig. 5*B*, *yellow stars* indicate wounds; see supplemental Movie). Immediately after the confluent cell layers were scratched, GFP-JRAB fluorescence intensity was high at thick actin bundles in cells at the wound edge, whereas fluorescence intensity was low at adhesion sites (Fig. 5, *B* and *C*, 0 h, *red dots* on *yellow line* in *photograph*, *red arrows* in *graph*). After wound closure, however, fluorescence intensity decreased at new cell-cell adhesion sites where the free edges of the cells from opposite sides of the wound made contact (Fig. 5, *B* and *C*, 2 h 34 min, *red dots* on *yellow line* in *photograph*, *red arrows* in *graph*). These results suggest that the change in JRAB behavior is associated with the

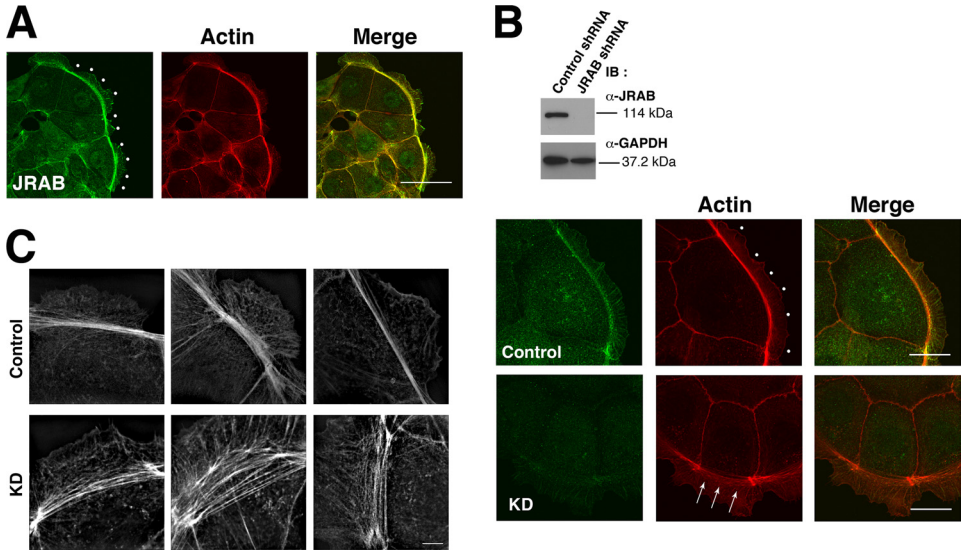

FIGURE 4. **Effect of JRAB on the actin bundle along the free border in MTD-1A cells.** *A,* localization of JRAB at the free border (*dots*). *Bar,* 50 μm. *B,* effect of JRAB knockdown on the actin bundle along the free border. *Top panel,* expression levels of JRAB and GAPDH in the cells. *Bottom panel,* confocal microscopic image of the actin bundle along the free border (*arrows* and *dots*) in JRAB-knockdown and control cells. *IB,* immunoblotting. *Bar,* 20 μm. *C,* super-resolution image of the actin bundle along the free border in JRAB-knockdown and control cells. *Bar,* 5 μm. The results shown are representative of at least three independent experiments.

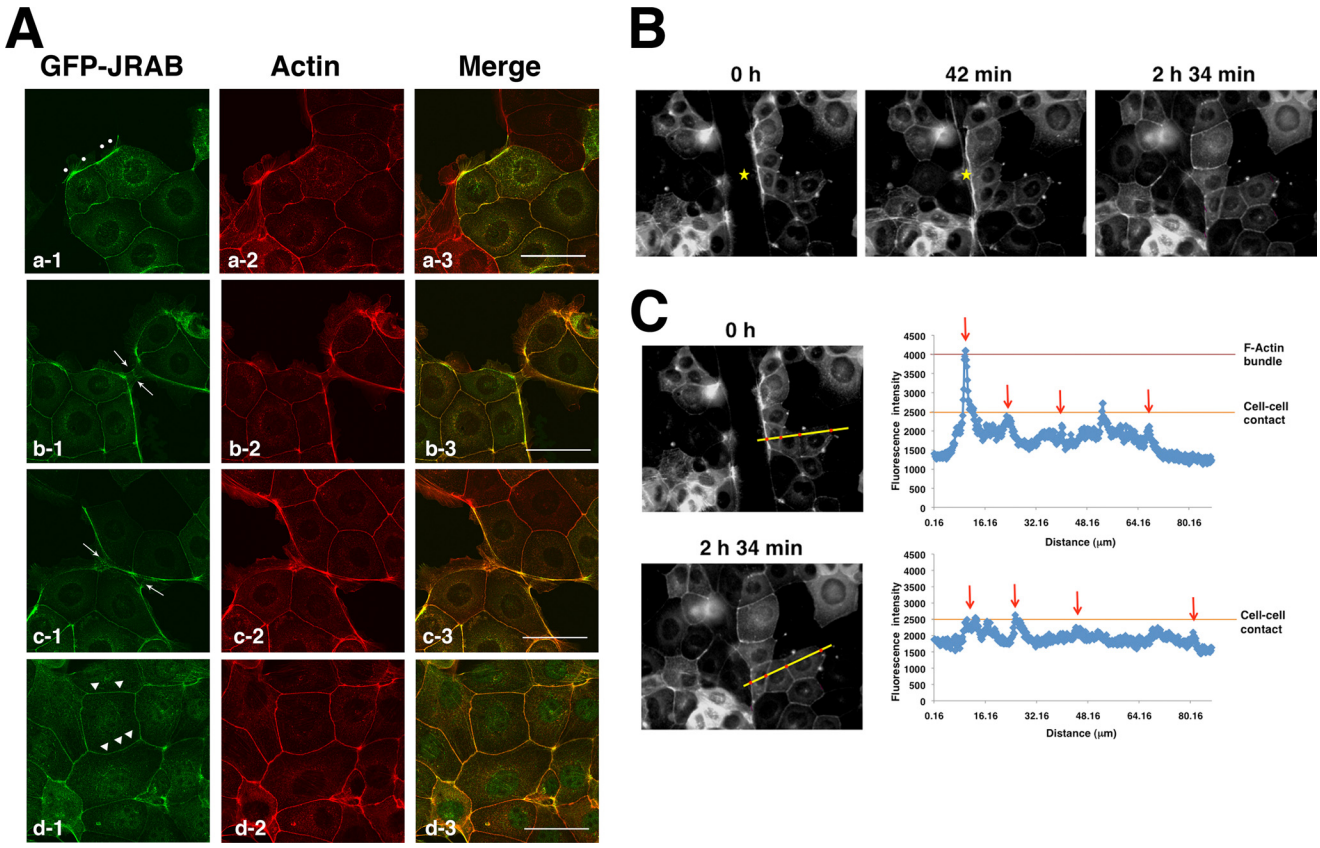

FIGURE 5. **Behavior of JRAB changes throughout epithelial junctional development.** *A,* behavior of GFP-JRAB in MTD-1A cells during junctional development. MTD-1A cells expressing GFP-tagged JRAB were fixed and processed for double fluorescence. *Dots* indicate arcs; *arrows* indicate cell-cell contact sites; *arrowheads* indicate well developed cell-cell adhesion sites. *Bar,* 50 μm. *B* and *C,* confluent monolayers of MTD-1A cells expressing GFP-JRAB were scratched. After wounding, cells at the wound edge were observed using a time-lapse microscope. *Yellow stars* indicate wounds. The *graph* indicates the intensity of GFP-JRAB on the *yellow line*. The *red arrows* indicate the intensity of *red dots* on the *yellow line*. The results shown are representative of at least three independent experiments.

reorganization of the actin cytoskeleton during epithelial junctional development.

Conformational Change of JRAB in Adaptation to the Different Phases of Junctional Development—In contrast to JRAB, the fluorescence of GFP-Rab13 appeared in a vesicle-like pattern scattered throughout the cytoplasm (Fig. 6*A*). GFP-Rab13 was also detected at cell-cell adhesion sites, but it was not detected in arcs. The distribution of GFP-Rab13DA (dominant-active) was similar, whereas GFP-Rab13DN (dominant-negative) was homogeneously distributed throughout the cytoplasm (Fig.

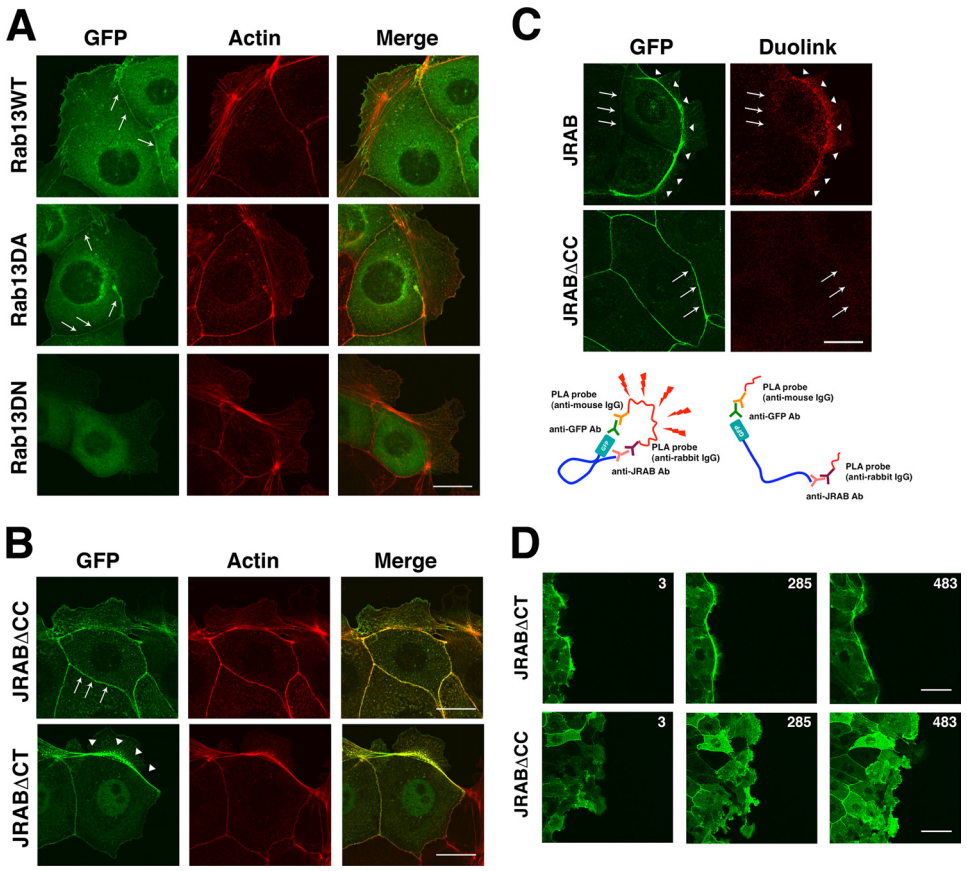

FIGURE 6. **Rab13-dependent conformational change of JRAB determines its localization.** *A,* localization of GFP-Rab13 and its mutants. *Bar,* 20 μm. *B,* localization of GFP-JRAB mutants. *Bar,* 20 μm. *C,* Duolink *in situ* PLA assay. MTD-1A cells expressing GFP-JRAB or GFP-JRABΔCC were subjected to the Duolink *in situ* PLA. *Arrowheads* indicate arcs; *arrows* indicate cell-cell adhesion sites. *Bar,* 20 μm. The schematic illustrates the principle of the Duolink *in situ* PLA. The results shown are representative of at least three independent experiments. *D,* confluent monolayers of MTD-1A cells expressing GFP-JRABΔCT or GFP-JRABΔCC were scratched. After wounding, cells at the wound edge were observed using a time-lapse microscope. Each image was captured at the indicated time (min).

6*A*). Previously, we found that GTP-Rab13 binds to JRAB via the C-terminal (CT) region that follows the CC domain and that the CH+LIM domain engages in an intramolecular interaction with the CC domain (30). We also developed the JRABΔCC mutant, lacking the CC domain (open form), and the JRABΔCT mutant, lacking the Rab13-binding CT domain (closed form) (30). To understand the role of JRAB conformational changes, we examined the distributions of these mutants. GFP-JRABΔCT could be clearly detected in the arcs (Fig. 6*B*), as was GFP-JRAB (see Fig. 5*A*). In contrast, GFP-JRABΔCC preferentially localized to cell-cell adhesion regions but could only be faintly detected at the arcs (Fig. 6*B*). We also found that actin bundle formation at the free border is more prominent in the cells expressing JRABΔCT than that in the cells expressing JRABΔCC (Fig. 6*B*). This observation was supported by the data using HEK293 cells; overexpression of JRAB induced actin bundles within the cells, although they disappeared by coexpression of Rab13DA with JRAB (supplemental Fig. 2). Additionally, we analyzed the conformational change of JRAB in the cells using Duolink *in situ* PLA. This assay system consists of a pair of oligonucleotide-labeled secondary antibodies (PLA probes) (34). A signal is generated only when the two PLA probes bind in close proximity. We used a rabbit anti-JRAB antibody, raised against GST-JRAB-C, and mouse anti-GFP antibody. (see Fig. 6*C*, *schema*) We observed a strong signal at the arc but not at cell-cell adhesion sites in MTD-1A cells expressing GFP-JRAB (Fig. 6*C*). In contrast, no signal was observed at cell-cell adhesion sites of cells expressing GFP-JRABΔCC. Next, we examined the significance of the conformational change of JRAB during wound closure. The thick actin bundles are generated in the front cells at the wound edge, like police who lock arms during crowd control, and it plays a crucial role in the cooperative epithelial sheet migration (35). As described above, GFP-JRAB fluorescence intensity was high at thick actin bundles in edge cells (see Fig. 5*B*). GFP-JRABΔCT was also concentrated at thick actin bundles in cells at the wound edge and maintained the front line during wound closure (Fig. 6*D*). In contrast, the cell expressing GFP-JRABΔCC did not produce the thick actin bundles at the free edge (see Fig. 6*B*), and uncoordinated lamellipodia were induced toward the wound, disturbing the front line and coordinated epithelial sheet migration for wound closure (Fig. 6*D*). These results suggest that the conformational change of JRAB is also related to the quality control of the actin cytoskeleton.

In summary, JRAB along the arcs is "closed" in the absence of Rab13, whereas JRAB associates with Rab13 at cell-cell adhesion sites, resulting in a conformational change to the "open" state. These findings suggest that JRAB behaves in different ways during different phases of epithelial junctional development; these distinct behaviors, mediated by a conformational

change in JRAB, lead to the creation of a new cellular environment, and the disturbance of this conformational change impedes the junctional formation process.

Quality Control of F-actin Reorganization by JRAB in the Epithelial Cells—We next examined how JRAB regulates the dynamics of the actin cytoskeleton in MTD-1A cells. For this purpose, we performed Ca^{2+} switch assay, because actin dynamics during the disassembly and assembly of the cells could be analyzed in detail using this method (8, 9, 36, 37). When the Ca^{2+} concentration in the medium was changed to low, the cell-cell adhesion disassembly is induced (8). Ca^{2+} depletion resulted in dramatic changes of F-actin structure in MTD-1A cells from the cell-cell contacts under normal Ca^{2+} medium into subapical ring-like structures (Fig. 7*A*). GFP-JRAB was concomitantly translocated from the cell-cell adhesion sites to these ring structures (Fig. 7*A*). When the cells expressing GFP-JRABΔCT were cultured in the low Ca^{2+} medium, GFP-JRABΔCT was also translocated to the actin rings (Fig. 7*B*). However, the size of actin rings was very small compared with that observed in the GFP and GFP-JRAB-expressing cells, suggesting that GFP-JRAB may affect F-actin contraction necessary for the formation of the ring structure and that the ability of JRABΔCT is more potent than JRAB. Ivanov *et al.* (8) reported that non-muscle myosin II plays a role in the F-actin ring contraction and is important for the junctional disassembly. Consistently, addition of blebbistatin, myosin II inhibitor, to the cells expressing GFP-JRABΔCT completely blocked the formation of actin rings (Fig. 7*C, panel a*). Moreover, addition of Y-27632, ROCK inhibitor, to the cells completely inhibited the formation of the actin ring (Fig. 7*C, panel b*). These results support that GFP-JRABΔCT may stimulate the myosin II activity through the Rho pathway. In contrast, when the cells expressing GFP-JRABΔCC were cultured in the low Ca^{2+} medium, F-actin maintained at the cell-cell adhesion sites could be observed (Fig. 7*B*). E-cadherin and claudin-1 also mostly remained at the cell-cell adhesion sites even after a 2-h Ca^{2+} depletion (Fig. 7*D, panel a*). Similarly, jasplakinolide, the inhibitor of actin depolymerization, prevented the cell-cell adhesion disassembly (Fig. 7*D, panel b*), as reported previously (8). These results suggest that GFP-JRABΔCC may maintain the cell-cell adhesion through F-actin stabilization. As shown in Fig. 3*C*, CH+LIM inhibited the F-actin depolymerization and stabilized it. However, this stabilizing activity of CH+LIM was inhibited by the C domain (Fig. 7*E*), suggesting that the activity may be masked by the intramolecular interaction of JRAB and released in the mutant of the open form. Moreover, the cells expressing GFP-JRABΔCC exhibited higher TER than GFP and GFP-JRABΔCT (Fig. 7*F*) after the junctional maturation, strengthening the model that the JRAB-induced F-actin stabilization is important for the generation and maintenance of stable cell-cell adhesion.

As to junctional assembly after Ca^{2+} restoration, actin polymerization and myosin II are reported to play differential roles and myosin II activity is crucial for tight junction (TJ) formation but not for adherens junctions formation (9). Our biochemical analyses as described above suggested that JRAB is not involved in actin polymerization. However, from the results in the Ca^{2+}-depletion experiments, JRAB may play a role in the regulation of actin dynamics driven by myosin II activity, and JRABΔCT may exhibit a prominent relationship to the activity. Then we next examined whether myosin II activity mediated by JRABΔCT is involved in junctional assembly. In the cells expressing JRABΔCT, perijunctional actin ring was formed at 30 min after Ca^{2+} restoration, and JRABΔCT was also concentrated at the ring (Fig. 7*G*). After 2 h, actin was localized to the cell-cell adhesion sites, and the mature junction was completely recovered during 24 h (Fig. 7*G*), which is confirmed by the staining of claudin-1 (Fig. 7*H*). In contrast, addition of blebbistatin to the medium inhibited the actin ring formation (data not shown), and even after 24 h of Ca^{2+} restoration, claudin-1 was not completely recovered to the cell-cell adhesion sites in the cells expressing GFP-JRABΔCT (Fig. 7*H*).

Relationship between JRAB and Actinins during Junctional Development—Finally, we examined the relationship between JRAB and actinins. Actinin-1/4 localized to the thick actin bundles along the free border and cell-cell adhesion sites (Fig. 8*A*). Previously, we showed that GTP-Rab13 enhances the affinity of JRAB to actinin-4 (26). Consistent with this, in coimmunoprecipitation assays actinin-4 bound JRABΔCC, whereas a lesser amount of actinin-4 bound JRABΔCT (Fig. 8*B, panel a*). Moreover, JRABΔCC bound actinin-1 much more strongly than JRABΔCT (Fig. 8*B, panel a*). In MTD-1A cells expressing GFP-JRABΔCC, actinin-4 as well as actinin-1 was prominent at cell-cell adhesion sites, rather than arcs (Fig. 7*B, panel b*). In contrast, when GFP-JRABΔCT was expressed in the cells, actinin-1 and -4 were prominent at the arcs (Fig. 7*B, panel b*). These results suggest that JRAB interacts with these actin-binding proteins at cell-cell adhesion sites, whereas JRAB colocalizes with these proteins, but does not interact with them, in arcs.

We also analyzed the effect of JRAB-actinin-4 interactions on actin cross-linking. Because both JRAB and actinin-4 possess bundling activity, we used JRAB-MID1, which interacts with actinin-4 but does not have cross-linking activity. In low speed cosedimentation assays using F-actin, MID1 inhibited the bundling activity of actinin-4 (Fig. 8*C, panel a*). Previously, we showed that actinin-4 binds to JRAB through its C terminus (aa 552–912), which does not exhibit bundling activity by itself (26). This C-terminal region of actinin-4 inhibited the bundling activity of JRABΔCC (Fig. 8*C, panel b*). These results suggest that JRAB and actinin-4 cooperatively stimulate F-actin cross-linking to produce the thick F-actin bundles in arcs, whereas JRAB and actinin-4 inhibits their cross-linking activities each other through their direct interactions to generate thin cortical actin bundles at the cell-cell adhesion sites.

DISCUSSION

Cell-cell adhesion is crucial for development and tissue homeostasis and is a fundamental and dynamic process underlying multiple cellular behaviors (1, 2). During the processes leading to cell-cell adhesion, dynamic reorganization of the actin cytoskeleton occurs in coordination with the phases of junctional development (10). At the initiation of a cell-cell junction, F-actin is actively bundled at the cellular edge along the free border, which will make contact with another cell and form the cell-cell junction; such bundles produce the force required to pull cells toward their neighbors, allowing them to adhere

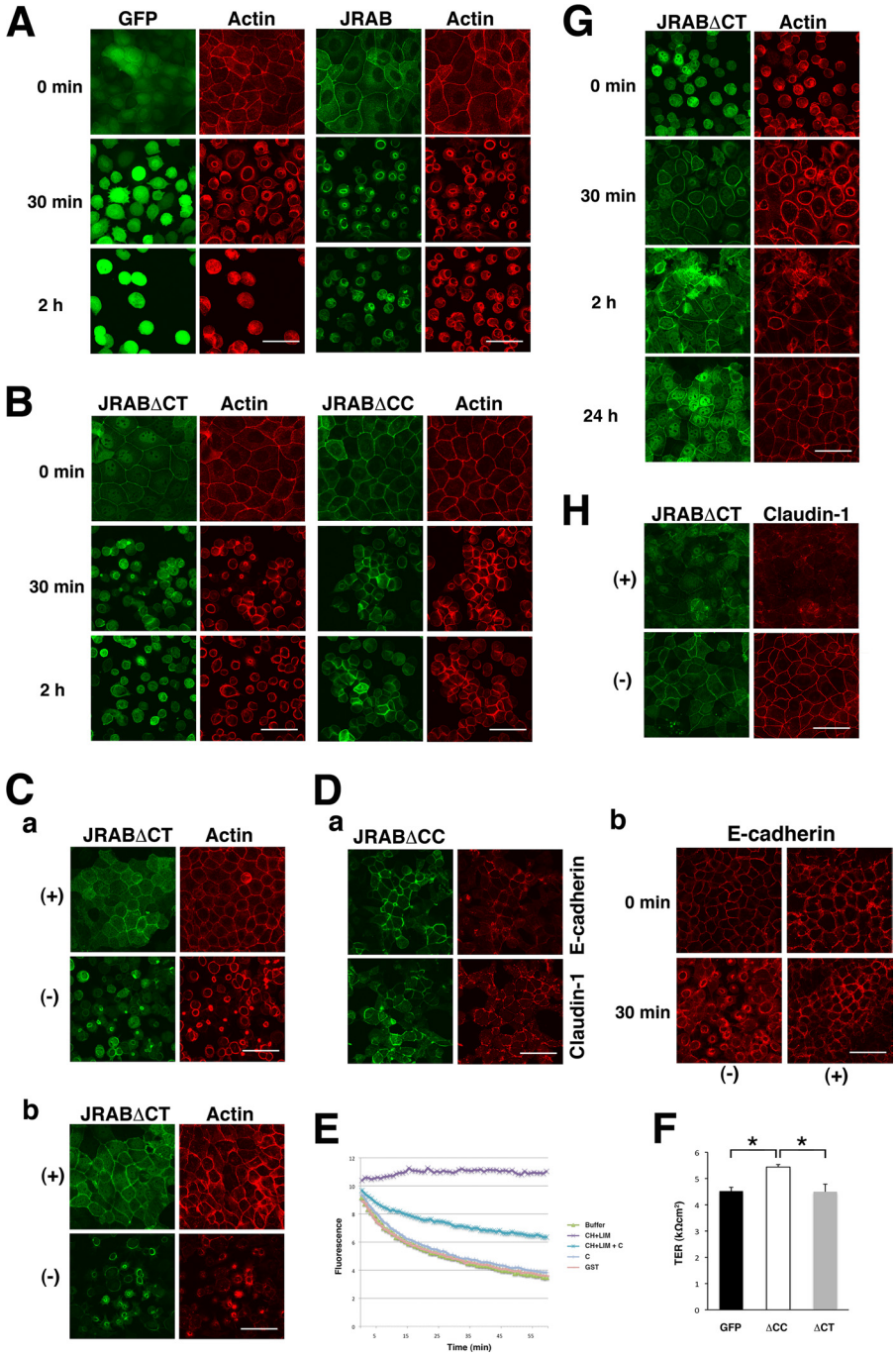

FIGURE 7. **Effect of JRAB on actin dynamics in MTD-1A cells.** *A,* association of GFP-JRAB with junctional disassembly in Ca^{2+}-starved MTD-1A cells. MTD-1A cells expressing GFP or GFP-JRAB were cultured in low Ca^{2+} medium for the indicated times and then fixed and processed for double fluorescence. *Bar,* 50 μm. *B,* effect of GFP-JRAB mutants on actin dynamics during junctional disassembly. MTD-1A cells expressing GFP-JRABΔCT or GFP-JRABΔCC were cultured in low Ca^{2+} medium for indicated times, and then fixed and processed for double fluorescence. *Bar,* 50 μm. *C,* blebbistatin and Y-27632 prevent reorganization of apical F-actin into ring-like structures leading to junctional disassembly in MTD-1A cells expressing GFP-JRABΔCT. The cells expressing GFP-JRABΔCT were preincubated in low Ca^{2+} medium containing (*panel a*) blebbistatin (50 μM) or (*panel b*) Y-27632 (20 μM) for 1 h, followed by 30 min-incubation in low Ca^{2+} medium containing the same concentration of each inhibitor. *Bar,* 50 μm. *D,* stabilization of F-actin in Ca^{2+}-depleted cells expressing GFP-JRABΔCC. *Panel a,* MTD-1A cells expressing GFP-JRABΔCC were incubated in low Ca^{2+} medium for 2 h, followed by fixation and processing for double fluorescence. Localization of E-cadherin or claudin-1 was determined by immunolabeling. *Panel b,* MTD-1A cells expressing GFP were preincubated in low Ca^{2+} medium containing jasplakinolide (2 μM) for 1 h, followed by incubation in low Ca^{2+} medium containing the same concentration of jasplakinolide. *Bar,* 50 μm. *E,* effect of the intramolecular interaction of JRAB on its F-actin stabilizing activity. The CH+LIM domain was incubated with pyrene-labeled F-actin in the presence or absence of GST-C, and fluorescence was monitored. The results shown are representative of three independent experiments. *F,* GFP-JRABΔCC increased TER in the monolayered MTD-1A cells. *Asterisks* indicate the statistical significance (*left panel*, $p = 0.042$; *right panel*, $p = 0.038$). *G,* GFP-JRABΔCT is involved in reorganization of F-actin structures associated with junctional assembly. After Ca^{2+} depletion for 3 h, MTD-1A cells expressing GFP-JRABΔCT were incubated in normal Ca^{2+} medium for indicated times. The cells were fixed and processed for double fluorescence. *H,* activity of myosin II is required for junctional assembly mediated by GFP-JRABΔCT. After Ca^{2+} depletion, MTD-1A cells expressing GFP-JRABΔCT were preincubated in low Ca^{2+} medium containing blebbistatin (50 μM) for 30 min, followed by a 24-h incubation in normal Ca^{2+} medium containing the same concentration of blebbistatin. The cells were fixed and processed for double fluorescence.

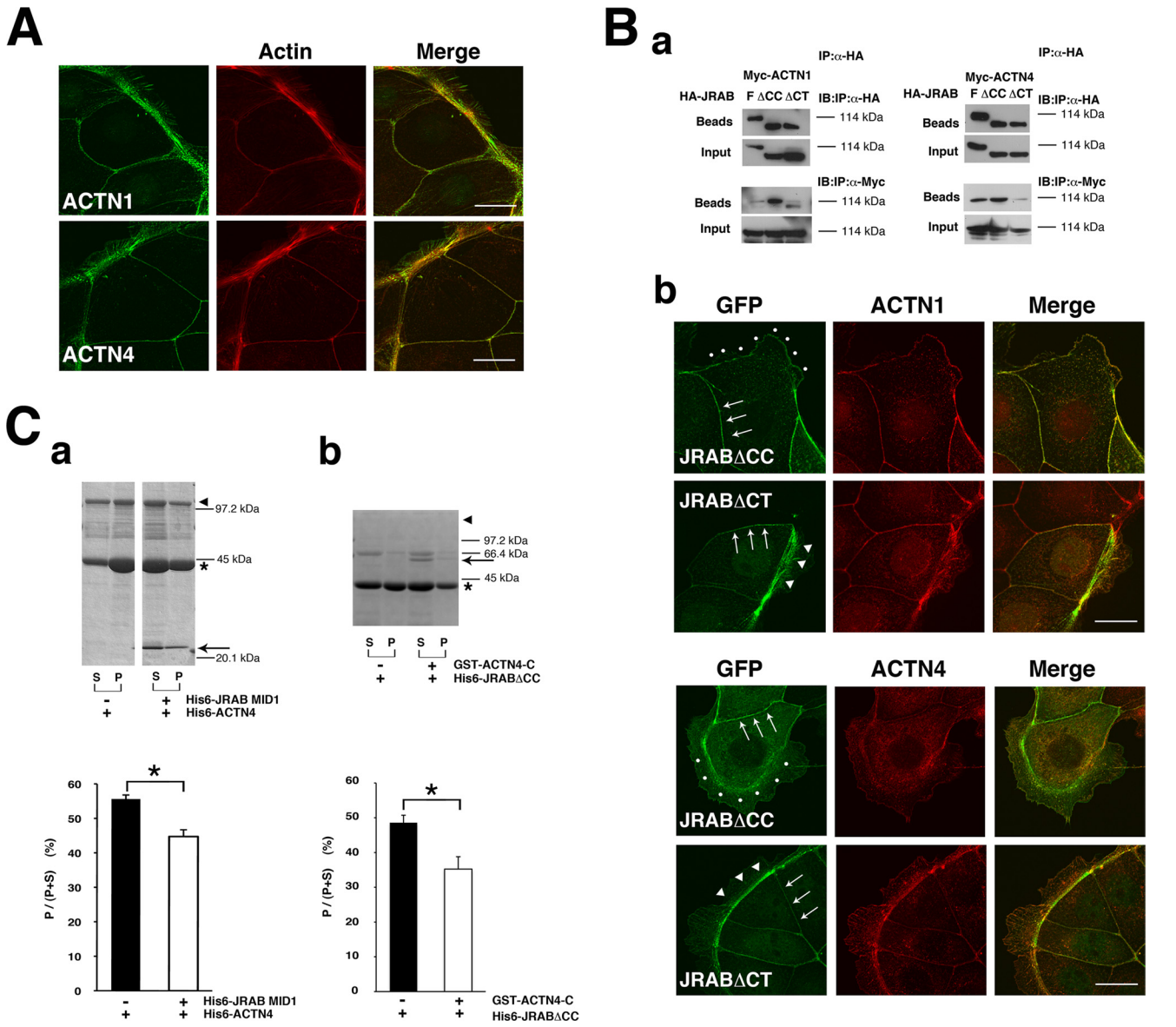

FIGURE 8. **Relationship between JRAB and actinins during junctional development.** *A,* JRAB-binding partners, actinin-1 and actinin-4, were localized to thick actin bundles along the free border as well as cell-cell adhesion sites. Cells were double-stained with rhodamine-phalloidin and either anti-actinin-1 or anti-actinin-4 antibody. *Bar,* 20 μm. *B, panel a,* HEK293 cells expressing HA-JRAB or its mutants and Myc-actinin-1 or -actinin-4 were lysed and subjected to immunoprecipitation (*IP*) assays using anti-HA antibodies. *IB*, immunoblot. *Panel b,* localization of JRAB mutants and actinins at the free border and cell-cell adhesion sites. *Arrowheads* indicate arcs; *dots* indicate free edges without an arc; *arrows* indicate cell-cell adhesion sites. *Bar,* 20 μm. *C, panel a,* F-actin cross-linking assay for actinin-4 and MID1. *Panel b,* F-actin cross-linking assay for JRABΔCC and actinin-4-C. *Asterisks* indicate actin; *arrowheads* indicate His_6-actinin-4 or His_6-JRABΔCC; *arrows* indicate His_6-JRAB-MID1 or GST-actinin-4-C. The results shown are representative of three independent experiments. The *graphs* show the ratio of actin in the pellet *versus* total actin in the pellet and supernatant ($P/(P+S)$) ($n = 3$). *Asterisks* indicate the statistical significance ($p = 0.032$ in *panel a* and $p = 0.009$ in *panel b*).

closely after cell-cell contacts are formed (35). During the maturation of cell-cell adhesion, actin fibers at cell-cell contacts become static, rather than dynamic, to maintain stable adhesion (38). Thus, cells need to spatiotemporally regulate the qualities of F-actin; many factors, including transmembrane adhesion molecules, submembrane plaque proteins, actin-binding proteins, and signal transduction molecules such as Rho family small G proteins, are involved in this regulation. To contribute to the spatiotemporal regulation of actin cytoskeletal organization, these molecules must be transported to their respective functional sites by vesicular trafficking. Thus, vesicle trafficking and organization of the actin cytoskeleton are intimately linked. However, it is unclear which molecules link these two systems, allowing the effective development of cell-cell adhesion. In this study, we focused on Rab13, a member of the Rab family small G proteins, which is a general regulator of vesicular trafficking, and its effector; we attempted to elucidate the roles of these proteins in linking trafficking with cytoskeletal organization.

Previously, we identified JRAB as an effector of Rab13 and showed that Rab13-JRAB regulates the vesicular transport of the TJ adhesion molecules occludin and claudin to the cell surface, resulting in the formation of strong cell-cell contacts (22, 24, 25). Vesicles containing Rab13 and adhesion molecules must be tethered to the PM, probably via the Rab13-JRAB interaction. Upon maturation of cell-cell adhesion sites, the zone of

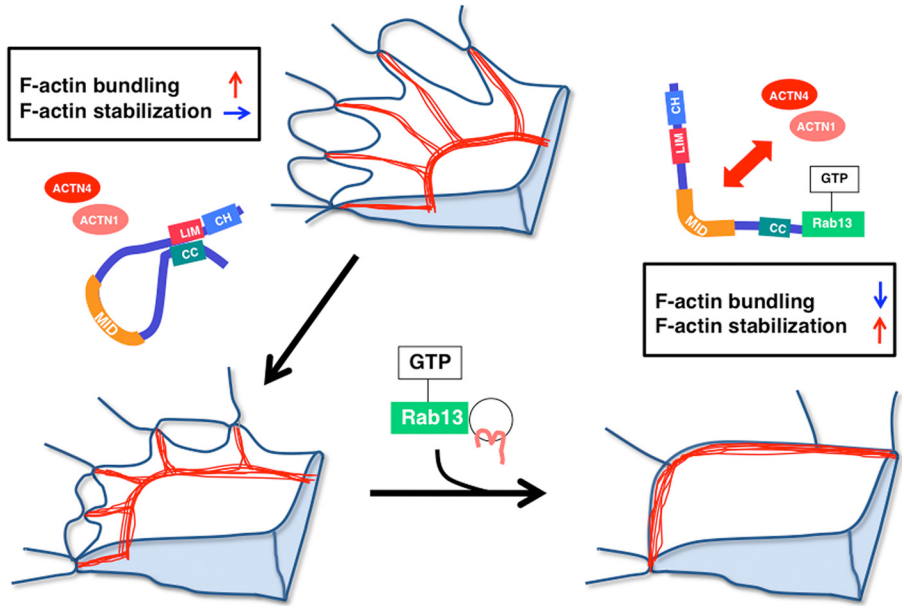

FIGURE 9. **Summary and model.** The schema is adapted from Ref. 10 to present our model. F-actin is shown in *red*.

interaction between Rab13 and JRAB gradually spreads inward from the edge of the free border as the region of the cell-cell contact expands. According to this scenario, the transport of adhesion molecules should be accompanied by the spatiotemporal regulation of actin cytoskeletal dynamics at the free border and at sites of cell-cell adhesion, and both processes may be simultaneously coordinated by Rab13-JRAB. In our previous report, we identified actinin-4, a well known actin-binding protein, as a JRAB-binding partner (26). In this report, we biochemically characterized each domain of JRAB and showed that JRAB binds to F-actin directly, and can both form F-actin bundles and stabilize F-actin by itself. We identified actinin-1 as a new JRAB-binding partner in addition to actinin-4, and determined which region of JRAB is necessary for binding the actinin proteins. JRAB-binding sites for actinin-1/4 and F-actin are separable, indicating the JRAB directly regulates organization of the actin cytoskeleton in an actinin-independent manner and also regulates it in an actinin-dependent manner. Our previous study showed that activated Rab13 causes JRAB to change its conformation from closed to open (30). Taking advantage of JRAB mutants that mimic these states, we found that JRAB plays a dual role in the quality control of F-actin and that its conformational change is necessary to fulfill the functions. We have analyzed using the Ca^{2+}-switch assay the functions of JRAB in the actin dynamics. We have first found that JRABΔCT affects the formation of the actin ring-like structure during junctional disassembly through the Rho-ROCK-myosin II pathway. We have also found that JRABΔCT is involved in the TJ formation through its effect on myosin II activity. When a single cell is contacting with its neighboring cells, a large actin ring structure could be observed. The ring could have tension to allow cells to form firm junctions precisely. It is not clear whether this actin-rich structure has similar properties to the one that we observed in Ca^{2+}-depleted cells; however, JRAB concentrates in both structures. From these data, JRAB, especially closed form, may be involved in producing tension, which is needed for junctional development. In contrast, JRABΔCC maintains the TJ through F-actin stabilization. Moreover, we presented the data that the interaction between JRAB and actinin-1/4 suppresses F-actin cross-linking activity, whereas the intramolecular interaction of JRAB inhibits its F-actin stabilizing activity. From these results, we favor a new model of the mode of action of JRAB on the actin dynamics during epithelial junctional development (Fig. 9). During initial adhesion between migrating cells, closed JRAB accelerates the formation of thick actin bundles at the free border, in cooperation with actinin-1/4. Subsequently, JRAB changes its conformation from closed to open, in a manner that depends on an interaction with GTP-Rab13. The open form of JRAB then interacts with actinin-1 or -4 at mature cell-cell adhesion sites. The interaction between open JRAB and actinin-1/4 suppresses their actin bundling activities; meanwhile, open JRAB activates the stabilization of F-actin via release of CH+LIM, leading to establishment and maintenance of stationary cell-cell adhesions. In summary, JRAB participates both in initiating adhesive contacts and in maturing and maintaining the contacts. Moreover, the conformational change of JRAB, which is under tight spatiotemporal control, plays a crucial role in the progression of these sequential processes.

Many questions remain unanswered as follows. Which signal cascade causes Rab13 activation to transport cell adhesion molecules and regulate JRAB function at cell-cell adhesion sites? What events occur downstream of the conformational change of JRAB? As to the latter question, we could get a hint concerning the relationship between JRAB and Rho family small G proteins from this study. Proteomic analyses using mass spectrometry have indicated that human JRAB is phosphorylated at multiple sites (39); the individual phosphorylation sites are involved in the development of lung cancer, early differentiation of human embryonic stem cells, or mitosis. Identifying the roles of such additional modifications could be the clue to our questions. Further studies will be required to obtain a detailed

picture of epithelial junctional development and its regulation by the Rab13-JRAB system.

Acknowledgments—We thank the members of our laboratory, M. Ikeda (Bio-Rad), and Y. Oikawa (Nikon Instec, Ltd.) for their assistance. We also thank Dr. Issei Imoto (University of Tokushima) for helping with the statistical analyses.

REFERENCES

1. Gumbiner, B. M. (1996) Cell adhesion. The molecular basis of tissue architecture and morphogenesis. *Cell* **84,** 345–357
2. Gumbiner, B. M. (2005) Regulation of cadherin-mediated adhesion in morphogenesis. *Nat. Rev. Mol. Cell Biol.* **6,** 622–634
3. Tsukita, S., Tsukita, S., Nagafuchi, A., and Yonemura, S. (1992) Molecular linkage between cadherins and actin filaments in cell-cell adherens junctions. *Curr. Opin. Cell Biol.* **4,** 834–839
4. Tsukita, S., Furuse, M., and Itoh, M. (2001) Multifunctional strands in tight junctions. *Nat. Rev. Mol. Cell Biol.* **2,** 285–293
5. Takai, Y., Miyoshi, J., Ikeda, W., and Ogita, H. (2008) Nectins and nectin-like molecules. Roles in contact inhibition of cell movement and proliferation. *Nat. Rev. Mol. Cell Biol.* **9,** 603–615
6. Takai, Y., Ikeda, W., Ogita, H., and Rikitake, Y. (2008) The immunoglobulin-like cell adhesion molecule nectin and its associated protein afadin. *Annu. Rev. Cell Dev. Biol.* **24,** 309–342
7. Krendel, M. F., and Bonder, E. M. (1999) Analysis of actin filament bundle dynamics during contact formation in live epithelial cells. *Cell Motil. Cytoskeleton* **43,** 296–309
8. Ivanov, A. I., McCall, I. C., Parkos, C. A., and Nusrat, A. (2004) Role for actin filament turnover and a myosin II motor in cytoskeleton-driven disassembly of the epithelial apical junctional complex. *Mol. Biol. Cell* **15,** 2639–2651
9. Ivanov, A. I., Hunt, D., Utech, M., Nusrat, A., and Parkos, C. A. (2005) Differential roles for actin polymerization and a myosin II motor in assembly of the epithelial apical junctional complex. *Mol. Biol. Cell* **16,** 2636–2650
10. Yonemura, S., Itoh, M., Nagafuchi, A., and Tsukita, S. (1995) Cell-to-cell adherens junction formation and actin filament organization: similarities and differences between non-polarized fibroblasts and polarized epithelial cells. *J. Cell Sci.* **108,** 127–142
11. Vasioukhin, V., Bauer, C., Yin, M., and Fuchs, E. (2000) Directed actin polymerization is the driving force for epithelial cell-cell adhesion. *Cell* **100,** 209–219
12. Zhang, J., Betson, M., Erasmus, J., Zeikos, K., Bailly, M., Cramer, L. P., and Braga, V. M. (2005) Actin at cell-cell junctions is composed of two dynamic and functional populations. *J. Cell Sci.* **118,** 5549–5562
13. Etienne-Manneville, S., and Hall, A. (2002) Rho GTPases in cell biology. *Nature* **420,** 629–635
14. Iden, S., and Collard, J. G. (2008) Cross-talk between small GTPases and polarity proteins in cell polarization. *Nat. Rev. Mol. Cell Biol.* **9,** 846–859
15. Jaffe, A. B., and Hall, A. (2005) Rho GTPases. Biochemistry and biology. *Annu. Rev. Cell Dev. Biol.* **21,** 247–269
16. Nelson, W. J. (2009) Remodeling epithelial cell organization. Transitions between front-rear and apical-basal polarity. *Cold Spring Harb. Perspect. Biol.* **1,** a000513
17. Takai, Y., Sasaki, T., and Matozaki, T. (2001) Small GTP-binding proteins. *Physiol. Rev.* **81,** 153–208
18. Zerial, M., and McBride, H. (2001) Rab proteins as membrane organizers. *Nat. Rev. Mol. Cell Biol.* **2,** 107–117
19. Hutagalung, A. H., and Novick, P. J. (2011) Role of Rab GTPases in membrane traffic and cell physiology. *Physiol. Rev.* **91,** 119–149
20. Zahraoui, A., Joberty, G., Arpin, M., Fontaine, J. J., Hellio, R., Tavitian, A., and Louvard, D. (1994) A small Rab GTPase is distributed in cytoplasmic vesicles in nonpolarized cells but colocalizes with the tight junction marker ZO-1 in polarized epithelial cells. *J. Cell Biol.* **124,** 101–115
21. Marzesco, A. M., Dunia, I., Pandjaitan, R., Recouvreur, M., Dauzonne, D., Benedetti, E. L., Louvard, D., and Zahraoui, A. (2002) The small GTPase Rab13 regulates assembly of functional tight junctions in epithelial cells. *Mol. Biol. Cell* **13,** 1819–1831
22. Morimoto, S., Nishimura, N., Terai, T., Manabe, S., Yamamoto, Y., Shinahara, W., Miyake, H., Tashiro, S., Shimada, M., and Sasaki, T. (2005) Rab13 mediates the continuous endocytic recycling of occludin to the cell surface. *J. Biol. Chem.* **280,** 2220–2228
23. Nishimura, N., and Sasaki, T. (2009) Rab family small G proteins in regulation of epithelial apical junctions. *Front. Biosci.* **14,** 2115–2129
24. Yamamura, R., Nishimura, N., Nakatsuji, H., Arase, S., and Sasaki, T. (2008) The interaction of JRAB/MICAL-L2 with Rab8 and Rab13 coordinates the assembly of tight junctions and adherens junctions. *Mol. Biol. Cell* **19,** 971–983
25. Terai, T., Nishimura, N., Kanda, I., Yasui, N., and Sasaki, T. (2006) JRAB/MICAL-L2 is a junctional Rab13-binding protein mediating the endocytic recycling of occludin. *Mol. Biol. Cell* **17,** 2465–2475
26. Nakatsuji, H., Nishimura, N., Yamamura, R., Kanayama, H. O., and Sasaki, T. (2008) Involvement of actinin-4 in the recruitment of JRAB/MICAL-L2 to cell-cell junctions and the formation of functional tight junctions. *Mol. Cell. Biol.* **28,** 3324–3335
27. Otey, C. A., and Carpen, O. (2004) α-Actinin revisited: a fresh look at an old player. *Cell Motil. Cytoskeleton* **58,** 104–111
28. Oikonomou, K. G., Zachou, K., and Dalekos, G. N. (2011) α-Actinin. A multidisciplinary protein with important role in B-cell driven autoimmunity. *Autoimmun. Rev.* **10,** 389–396
29. Kitamura, T., Koshino, Y., Shibata, F., Oki, T., Nakajima, H., Nosaka, T., and Kumagai, H. (2003) Retrovirus-mediated gene transfer and expression cloning: powerful tools in functional genomics. *Exp. Hematol.* **31,** 1007–1014
30. Sakane, A., Honda, K., and Sasaki, T. (2010) Rab13 regulates neurite outgrowth in PC12 cells through its effector protein, JRAB/MICAL-L2. *Mol. Cell. Biol.* **30,** 1077–1087
31. Honda, K., Yamada, T., Hayashida, Y., Idogawa, M., Sato, S., Hasegawa, F., Ino, Y., Ono, M., and Hirohashi, S. (2005) Actinin-4 increases cell motility and promotes lymph node metastasis of colorectal cancer. *Gastroenterology* **128,** 51–62
32. Morita, S., Kojima, T., and Kitamura, T. (2000) Plat-E. An efficient and stable system for transient packaging of retroviruses. *Gene Ther.* **7,** 1063–1066
33. James, P., Halladay, J., and Craig, E. A. (1996) Genomic libraries and a host strain designed for highly efficient two-hybrid selection in yeast. *Genetics* **144,** 1425–1436
34. Söderberg, O., Gullberg, M., Jarvius, M., Ridderstråle, K., Leuchowius, K. J., Jarvius, J., Wester, K., Hydbring, P., Bahram, F., Larsson, L. G., and Landegren, U. (2006) Direct observation of individual endogenous protein complexes *in situ* by proximity ligation. *Nat. Methods* **3,** 995–1000
35. Gov, N. (2011) Cell mechanics. Moving under peer pressure. *Nat. Mater.* **10,** 412–414
36. Samarin, S. N., Ivanov, A. I., Flatau, G., Parkos, C. A., and Nusrat, A. (2007) Rho/Rho-associated kinase-II signaling mediates disassembly of epithelial apical junction. *Mol. Biol. Cell* **18,** 3429–3439
37. Ivanov, A. I., Bachar, M., Babbin, B. A., Adelstein, R. S., Nusrat, A., and Parkos, C. A. (2007) A unique role for nonmuscle myosin heavy chain IIA in regulation of epithelial apical junctions. *PLoS One* **2,** e658
38. Hidalgo-Carcedo, C., Hooper, S., Chaudhry, S. I., Williamson, P., Harrington, K., Leitinger, B., and Sahai, E. (2011) Collective cell migration requires suppression of actomyosin at cell-cell contacts mediated by DDR1 and the cell polarity regulators Par3 and Par6. *Nat. Cell Biol.* **13,** 49–58
39. Rahajeng, J., Giridharan, S. S., Cai, B., Naslavsky, N., and Caplan, S. (2010) Important relationships between Rab and MICAL proteins in endocytic trafficking. *World J. Biol. Chem.* **1,** 254–264